



Chapter 5: Regulation of Star Formation and the Evolution of Galaxies

Feedback models in galaxy simulations and probing their impact by cosmological hydrodynamic simulations

Kentaro Nagamine^{1,2,3} 

¹Theoretical Astrophysics Group, Department of Earth and Space Science,
Graduate School of Science, Osaka University
1-1 Machikaneyama-cho, Toyonaka, Osaka, 560-0043, Japan

²Department of Physics & Astronomy, University of Nevada, Las Vegas
4505 S. Maryland Pkwy, Las Vegas, NV 89154-4002, USA

³Kavli IPMU, The University of Tokyo, 5-1-5 Kashiwanoha, Kashiwa, Chiba, 277-8583, Japan
email: kn@astro-osaka.jp

Abstract. Feedback effects by supernovae (SNe) and active galactic nuclei (AGNs) are believed to be essential for galaxy evolution and shaping present-day galaxies, but their exact mechanisms on galactic scales and their impact on CGM/IGM are not well understood yet. In galaxy formation simulations, it is still challenging to resolve sub-parsec scales, and we need to implement subgrid models to account for the physics on small scales. In this article, we summarize some of the efforts to build more physically based feedback models, discuss about pushing the resolution to its limits in galaxy simulations, testing galaxy formation codes under the AGORA code comparison project, and how to probe the impact of feedback using cosmological hydrodynamic simulations via Ly α absorption and CGM/IGM tomography technique. We also discuss our future directions of research in this field and how we make progress by comparing our simulations with observations.

Keywords. cosmology: theory, galaxies: formation, galaxies: evolution, galaxies: ISM, galaxies: high-redshift, hydrodynamics

1. Introduction

It is widely accepted that feedback processes by SNe and AGNs regulate galaxy formation and evolution. The standard lore is that the AGN feedback suppresses star formation in massive galaxies at lower redshift, and the SN feedback in low-mass galaxies at higher redshift, hence causing the peak in the stellar-to-halo mass relation (Behroozi et al. 2013). In particular, many interesting physical processes take place in high-redshift galaxies as we summarize in a schematic diagram below (Fig. 1), and therefore they are good laboratories for testing feedback models. Low-metallicity gas falls into the dark matter halo via narrow, cold streams, providing abundant fuel for star formation (Kereš et al. 2005; Wright et al. 2021). At lower redshifts of $z \lesssim 2$, gas accretion switches to the hot accretion mode, and prominent cold flows are no longer observed in simulations (Faucher-Giguère et al. 2011; Nelson et al. 2016). The cosmic star formation rate density (SFRD) has a broad peak at $z \simeq 3 - 5$ (e.g., Nagamine et al. 2000; Nagamine et al. 2004, 2006; Kistler et al. 2009; Madau & Dickinson 2014), and the rising SFRD at high-redshift is driven by gravitational instability where dark matter halos and galaxies actively form (Schaye et al. 2010). Different emission lines such as Ly α , [C II], [O III] are expected

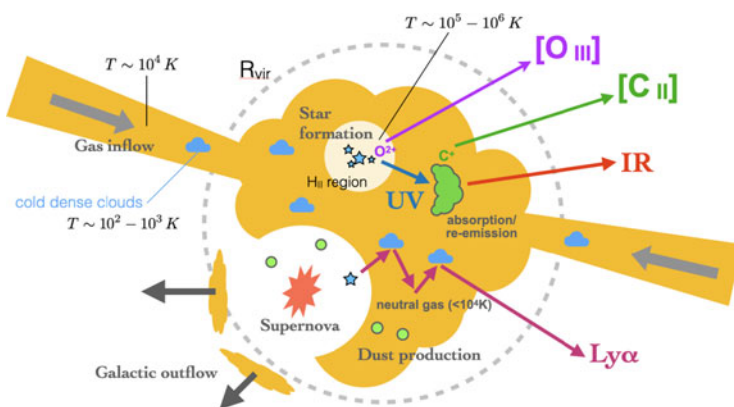


Figure 1. Schematic figure describing various physical processes in high-redshift galaxies. The gas flows into the dark matter halo via cold streams of $T \sim 10^4$ K, and later condenses into dense clouds with $T \sim 10^2 - 10^3$ K via radiative cooling. Once the stars form, the massive stars ionize the ISM around them and produce H II regions. The UV radiation from massive stars impinges on the surface of ISM and produces photo-dissociation regions (PDR), where infrared emission lines such as [C II] are emitted as a reprocessed radiation. These emissions from high- z galaxies have been computed using cosmological zoom-in hydrodynamic simulations (e.g., Arata et al. 2019; Katz et al. 2022). Prominent Ly α emissions are also observed from high- z galaxies. The massive stars die after several Myrs, and the gas is ejected as galactic outflows.

from high- z galaxies, and many of those lines have recently been observed by ALMA (e.g., Smit et al. 2018; Hashimoto et al. 2018, 2019), suggesting a very early onset of star formation at $z \sim 15$.

One of the important physical parameters to determine the radiative properties of high- z galaxies is the escape fraction f_{esc} of ionizing and ultra-violet (UV) photons. However, it is difficult to estimate f_{esc} observationally and only a handful of rough measurements have been made. Therefore, it would be desirable to predict f_{esc} for different types of galaxies directly from hydrodynamic simulations of galaxy formation (e.g., Cen 2003; Razoumov & Sommer-Larsen 2006; Gnedin et al. 2008; Wise & Cen 2009; Yajima et al. 2017). It requires accurate computations of ISM structure and hence a high-resolution to predict f_{esc} . Understanding the details of f_{esc} is also quite important for figuring out whether the reionization of the universe favors the ‘Early’ or ‘Late’ scenarios (e.g., Finkelstein et al. 2019; Naidu et al. 2020).

2. Feedback models in galaxy formation simulations

In the early cosmological hydrodynamic simulations, SN feedback was modeled with simple injection of thermal energy on large scales ($> \text{kpc}$) (Cen & Ostriker 1992; Katz 1992; Katz et al. 1996; Cen & Ostriker 1999). However, the injected thermal energy would be radiated away quickly in low-resolution simulation because the Sedov-Taylor phase of each SN (or collective superbubble) cannot be resolved in detail, i.e., the well-known overcooling problem. Therefore, effective models of SN feedback need to be developed, and several strategies have been taken in galaxy formation simulations; for example, (i) ignoring and bypassing the physics on unresolved scales; (ii) scaling up the energy dynamics to a resolvable scale by considering cumulative energies; or (iii) modeling the physics on unresolved scales via subgrid models.

As examples of method (i), the ‘delayed cooling’ model ignores the cooling for a short period of time after the SN event to make thermal feedback effective (Thacker & Couchman 2000; Stinson et al. 2006). The constant velocity wind model

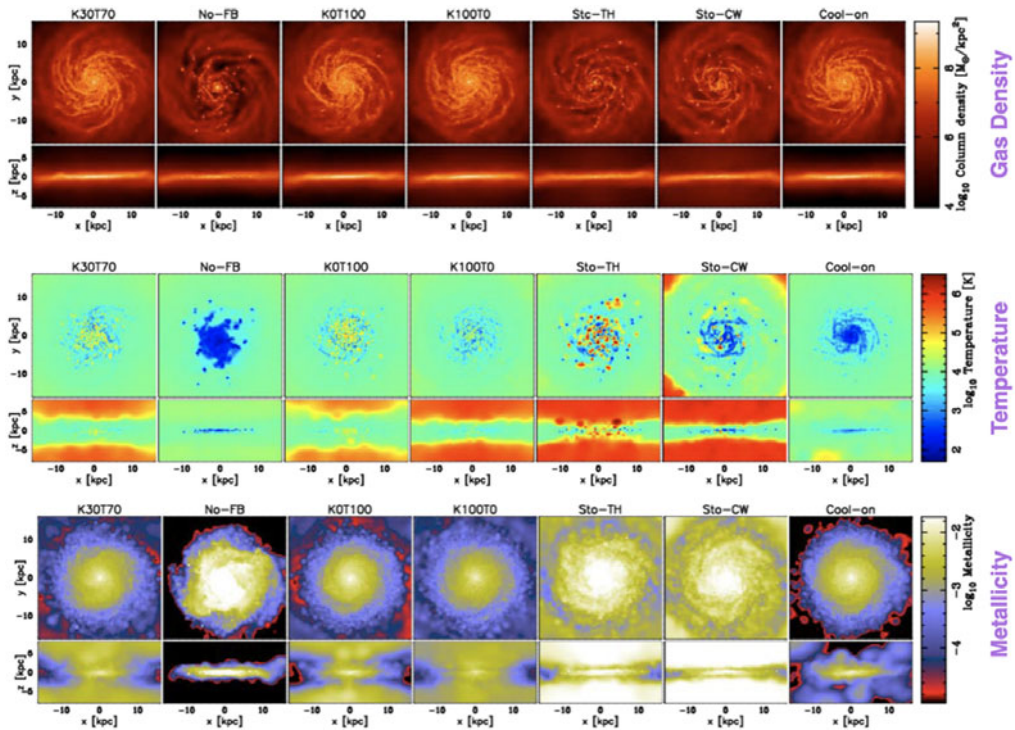


Figure 2. An example of testing SN feedback models in isolated galaxy simulations, showing projected gas density, mass-weighted temperature, and metallicity from top to bottom rows, respectively (Shimizu et al. 2019). In each row, the top panels show face-on view, and the lower panel shows the edge-on view.

of Springel & Hernquist (2003) stochastically kicks gas particles by turning off the hydro forces until the wind particles get out of the galaxies in a smoothed particle hydrodynamics (SPH) code. As an example of method (ii), ‘stochastic thermal feedback’ model increases the temperature of neighboring fluid elements by ΔT (Kay et al. 2003; Dalla Vecchia & Schaye 2012), so that the subsequent evolution of hot bubble can be solved by a hydro solver with efficient thermal feedback. But the choice of ΔT remains ad hoc and uncertain. As an example of method (iii), ‘multiphase ISM model’ treats single SPH particle as a multiphase gas, and the energy exchange between hot and cold phase is treated by a subgrid equilibrium model (Yepes et al. 1997; Springel & Hernquist 2003; Keller et al. 2014). Another model is injecting the terminal momentum of single SN explosion based on Sedov–Taylor solution (Kimm & Cen 2014; Hopkins et al. 2018). See Nagamine (2018) and Oku et al. (2022) for more discussions of different feedback treatments.

In Shimizu et al. (2019), we combined the delayed cooling model and kinetic feedback using the Sedov–Taylor self-similar solution in GADGET3–Osaka code. We show an example of testing different SN feedback models in Fig. 2. Here in the fiducial model (K30T70), 30% of the SN energy was injected as kinetic energy, and 70% as thermal energy following earlier work (e.g., Chevalier 1974; Durrer & Dalla Vecchia 2012). The cooling was temporarily shut off for the neighbor particles which received the thermal feedback energy. One can see a very clumpy, cold, dense gas distribution in the face-on gas distribution image of ‘No-feedback’ (No-FB) run, with no hot gas above the disk. If the fraction of thermal energy injection is increased, the spiral arms become more fluffy compared to the

Fiducial run. The ‘Stochastic thermal’ (Stc-TH) and ‘Stochastic constant wind velocity’ (Sto-CW) runs also have some clumpy knots in the disk, but the feedback effects above the disk is very strong with hot outflowing gas, hence over-enriching the CGM. If the cooling is turned on (‘Cool-on’ run), the heated gas by the feedback quickly cools back down and will not get out of the disk. Therefore the Cool-on run shows similar disk feature as the No-FB run. The Osaka feedback model by Shimizu et al. (2019) provided useful comparison of various SN feedback treatment, succeeded in the self-regulation of star formation and naturally produced galactic outflow, however, it did contain some unphysical treatment (e.g., turning the cooling off for effective thermal feedback).

In Oku et al. (2022), we went back to single SN remnant (SNR) and superbubble following the same spirit of earlier works (Chevalier 1974; Weaver et al. 1977; Tomisaka & Ikeuchi 1986; Ostriker & McKee 1988; Martizzi et al. 2015; Kim & Ostriker 2015; Kim et al. 2017), and investigated the metallicity dependence of the terminal moment of SN shell. Using the Eulerian hydrodynamic code ATHENA++, we extended the analytic solution of the SNR shell-formation time by (Kim & Ostriker 2015) to include the effect of metallicity, and obtained the analytic solution of the superbubble shell-formation time. We found a universal scaling relations for the time evolution of momentum and radius for a superbubble, when the momentum and time are scaled by those at the shell-formation time. We then developed a SN feedback model based on the ATHENA++ simulation results utilizing Voronoi tessellation around each star particle, and implemented it into the GADGET3-Osaka SPH code. We examined the mass/energy/metal loading factors and found that our stochastic thermal feedback model produced galactic outflow that carries metals above the galactic plane but with a weak suppression of star formation. Additional mechanical feedback further suppressed star formation and brought the simulation results into better agreement with the observations of the Kennicutt–Schmidt relation within the uncertainties of observed data. We argued that both thermal and mechanical feedback are necessary for the SN feedback model of galaxy evolution, especially in SPH simulations when an individual SN bubble is unresolved.

Some simulations have succeeded to push the resolution limit by focusing on low-mass galaxies. For example, Hu (2019) used the GADGET-3 SPH simulation to study SN feedback in a dwarf galaxy in a dark matter halo of virial mass $M_{\text{vir}} = 10^{10} M_{\odot}$, and achieved a resolution of $m_{\text{gas}} = 1 M_{\odot}$, and 0.3 pc for gravitational softening length and SPH smoothing length. Even with this resolution, some assumptions are still necessary (e.g. fraction of energy given as kinetic energy, and how many SPH particles receive the feedback energy). Nevertheless, they were able to simulate the formation of superbubbles of a few hundred parsecs in size, and how they break out of the galactic disk. Ma et al. (2020) simulated formation of dwarf galaxies in a halo of $M_{\text{vir}} = 3.7 \times 10^{10} M_{\odot}$ in reionization epoch using cosmological zoom-in simulation (FIRE-2 GIZMO), with a mass resolution of $m_{\text{gas}} = 100 M_{\odot}$ and a spatial resolution of \sim pc. They examined where the stars form in these high-redshift dwarf galaxies with respect to the superbubble walls, and found a large spatio-temporal variation in escape fraction of ionizing photons (cf. Wise & Cen 2009; Kimm & Cen 2014). As the mass resolution of simulations improve and approach ‘star-by-star’ simulation, one needs to devise a way to stochastically sample the IMF for the star formation model (Ploekinger et al. 2014; Hu 2019; Hirai et al. 2021), and its impact needs to be studied further for feedback as well.

3. The AGORA code comparison project

One of the ways to test galaxy formation codes is to perform a code comparison project such as the Santa Barbara cluster comparison project (Frenk et al. 1999), Aquila project (Scannapieco et al. 2012), nIFTy project (Knebe et al. 2015), and the AGORA project (Kim et al. 2014, 2016; Roca-Fàbrega et al. 2021). For example, the Santa Barbara

project highlighted different results from various hydrodynamic schemes and spurious entropy generation in SPH codes. This had a profound impact and led to the development of new SPH schemes that can resolve shocks better, such as the density-independent scheme (Saitoh & Makino 2013) or a more general formulation based on Lagrangian-based derivation (Springel & Hernquist 2002; Hopkins 2013). The Aquila comparison project found large code-to-code variations in galactic properties at $z=0$ such as the stellar mass, size, morphology and gas content. Their conclusion was that, due to different feedback prescriptions, the simulations could not yet uniquely predict galactic properties even when the dark matter halo assembly history were the same.

To make a more controlled comparison environment, the Assembling Galaxies of Resolved Anatomy (AGORA) project (†) started with a more rigorous calibration steps with common star formation recipe and the same Grackle cooling module (Smith et al. 2017) among all participating codes. With these common astrophysics setup, they were able to show more consistent behaviors between various codes (both SPH and AMR), and Kim et al. (2016) concluded that modern high-resolution galaxy formation simulations are more sensitive to input physics (e.g. feedback prescription) than to intrinsic differences in numerical schemes. Roca-Fàbrega et al. (2021) extended the comparison to cosmological zoom-in hydro simulations, and seven contemporary astrophysical simulation codes (ART-I, ENZO, RAMSES, CHANGA, GADGET-3, GEAR, and GIZMO) were compared. The comparison involved four methodical calibration steps, starting from a simple adiabatic run without cooling and star formation, then gradually adding steps to include cooling/heating and star formation. At the last fourth step, each code was asked to roughly reproduce the stellar mass of $10^9 M_{\odot}$ at $z=4$ in a halo which will become $10^{12} M_{\odot}$ at $z=0$, with code-dependent SN feedback recipes. With a physical resolution of $\lesssim 100$ pc at $z=4$, all codes *roughly* agree with each other on gas and stellar properties, but there were also interesting differences in the CGM temperature and chemical enrichment due to differences in feedback treatments (see Fig. 3). Their results also highlight the importance of further refining and constraining SN and AGN feedback models via comparison to various observations.

4. Probing the impact of feedback by cosmological simulations

It is also desirable to use large-scale cosmological hydro simulations to probe feedback in addition to isolated galaxies and zoom-in simulations. With large simulation box size and large galaxy samples, one can examine galaxy statistics such as galaxy stellar mass/luminosity functions or stellar-to-halo-mass ratio (see the contribution by R. Somerville to this proceedings). In addition to galaxies, we would also like to probe the distribution of diffuse baryons via absorption and emission lines. For example, the distribution of neutral hydrogen (HI) probed by the Ly α forest (e.g., Weymann et al. 1981; Cowie et al. 1995; Rauch 1998) reflects the strength of UV background radiation field as well as the local ionizing radiation, and we expect that the impact of feedback is imprinted in CGM/IGM (Cen et al. 1994; Hernquist et al. 1996; Miralda-Escudé et al. 1996; Zhang et al. 1997, 1998; Theuns et al. 2002; Cen et al. 2005; Kollmeier et al. 2006). The Ly α forest is one of the most powerful probes of cosmology, and it has been used to constrain cosmological parameters and matter power spectrum (Weinberg et al. 1998; Croft et al. 1998; McDonald et al. 2006; Iršič et al. 2017), as well as the mass of warm dark matter particles or neutrinos (e.g. Viel et al. 2005, 2013; Palanque-Delabrouille et al. 2015). This subject is also related to the so-called ‘Missing baryon problem’ (Cen & Ostriker 1999; Nicastro et al. 2005; Shull et al. 2012), where we still struggle to observationally account for the entire cosmic baryons.

† <https://sites.google.com/site/santacruzcomparisonproject/>

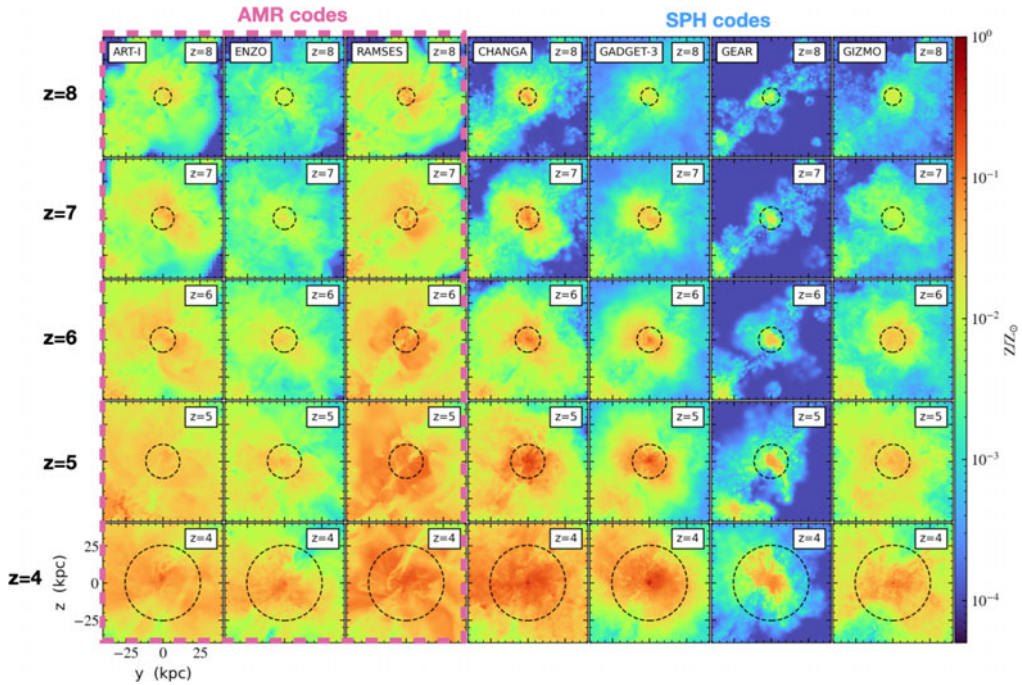


Figure 3. Comparison of projected (density-square-weighted) metallicity of seven different code from $z = 8$ to $z = 4$. Adapted from Fig. 18 of (Roca-Fàbrega et al. 2021).

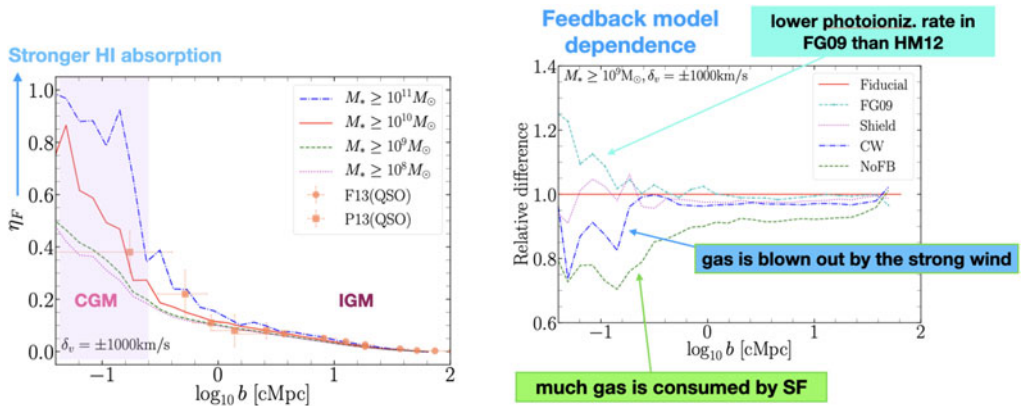


Figure 4. *Left:* $\text{Ly}\alpha$ flux contrast as a function of impact parameter from nearby galaxies. The data points are from Font-Ribera et al. (2013, orange filled circle; F13) and Prochaska et al. (2013, orange filled square; P13). *Right:* Relative difference in the flux contrast from the Fiducial model in runs with different feedback and UVB treatments. Both figures are from Nagamine et al. (2021).

The $\text{Ly}\alpha$ forest technique has recently been upgraded to IGM tomography, whereby one can generate 3D contour maps of HI density using more numerous star-forming galaxies as background sources than just using quasars sight-lines. A few groups have already demonstrated that this is possible (e.g., Lee et al. 2014, 2018; Cai et al. 2016; Mukae et al. 2020). Massive protoclusters have been discovered at $z = 2 - 3$ by the $\text{Ly}\alpha$ tomographic technique (Lee et al. 2016; Cai et al. 2017). In a more general sense, one can derive the correlation between galaxy overdensity and HI overdensity (Mukae et al. 2017; Liang et al. 2021). The scientific goals of IGM tomography are: (i) to characterize

the cosmic web at $z > 2$, (ii) to study the association between galaxies/AGNs and HI gas, and (iii) to identify protoclusters and voids in an *unbiased* manner.

As a pathfinder to the IGM tomography studies by the Subaru PFS (Takada et al. 2014; Greene et al. 2022) and upcoming observations by the JWST/TMT/ELT, Nagamine et al. (2021) investigated the impact of feedback on basic Ly α forest statistics by creating a light-cone data set at $z = 2 - 3$ and generating a mock Ly α forest data. They used five cosmological hydro simulations (GADGET3-0saka code) with different models of feedback and UVB treatment (comoving boxsize $L_{\text{box}} = 147.6$ Mpc, particle number $N = 2 \times 512^3$), and examined the 1D flux probability distribution function, 1D flux power spectrum, flux contrast vs. impact parameter from galaxies, and HI–galaxy cross-correlation. The flux contrast is defined as $\eta_F \equiv -\delta_F = 1 - \frac{F}{\langle F \rangle}$, where F is the transmitted flux ($F = e^{-\tau}$), and $\langle F \rangle$ is the average effective Ly α optical depth adjusted to the observed value (Becker & Bolton 2013). Higher η_F in the vicinity of galaxies means stronger absorption, i.e., more HI (left panel of Fig. 4). In other words, they found stronger HI absorption with decreasing impact parameter from galaxies, consistently with earlier simulation results (e.g., Bruscoli et al. 2003; Kollmeier et al. 2003, 2006; Meiksin et al. 2015; Turner et al. 2017; Meiksin et al. 2017; Sorini et al. 2018). Their simulation results showed overall agreement with current observational data, but with some interesting discrepancies of about 30% on small scales that are due to different treatments of feedback and UVB, or varying observational conditions (right panel of Fig. 4). The massive galaxies with $M_* \geq 10^{10} M_\odot$ contribute strongly to the flux contrast signal (left panel of Fig. 4), and the lower-mass galaxies with $M_* \approx 10^8 - 10^{10} M_\odot$ dilute the flux contrast signal from massive galaxies when the signal is averaged over the entire galaxy sample. The variations in η_F on scales of < 1 Mpc can be probed with future IGM tomography surveys with dense background source sampling by JWST/ELT/TMT. On large scales, the average flux contrast smoothly connects to the IGM level, supporting the spherical infall model and concordance Λ cold dark matter model, similarly to the results by Meiksin et al. (2017); Sorini et al. (2018). It is interesting to note that Sorini et al. (2020) found negligible impact of AGN feedback on the flux contrast, and they argued that stellar feedback is the primary driver determining the average physical properties of CGM at $z = 2 - 3$, which needs to be checked in other simulations with AGN feedback in the future (cf. Tillman et al. 2022).

In addition to HI distribution, metal distribution can also be probed by emission and absorption lines. For example, MEGAFLOW project has observed Mg II lines in both absorption and emission in galactic wind region of $z \sim 0.7$ galaxy (Zabl et al. 2020, 2021). Nelson et al. (2021) computed the resonantly scattered MG II emission from TNG50 simulation, and it seems that the simulated galaxies have somewhat steeper profile (declining faster with increasing radii) than the observed data points (their Fig. 3). But the currently observed sources are especially bright ones that are visible, so more comparison needs to be performed in the future with lower mass systems.

Interestingly, though, we find a similar trend in other emission lines, such as [C II] (Arata et al. 2020; Fujimoto et al. 2019), and Ly α (Zhang et al. 2020), where the simulated galaxies cannot account for the observed extended emission profiles. These discrepancies may have interesting implications for the feedback efficiencies (e.g., mass-loading factor of metals in galactic outflows; Pizzati et al. 2020), therefore requires further studies to constrain the efficiencies of chemical enrichment in CGM/IGM.

5. Summary

In this article, we reviewed various feedback treatments in galaxy simulations, and discussed our development of physically-based SN feedback models and the tests in the AGORA project using both isolated galaxies and zoom-in cosmological hydrodynamic

simulations. We argued that considering both thermal and kinetic modes is important for SN feedback at the current level of resolution ($\gtrsim 10$ pc). In our latest work, Oku et al. (2022) showed that the kinetic feedback suppresses star formation while stochastic thermal feedback drives strong metal outflows. Further studies on both small and large scales are important to constrain feedback effects in galaxy evolution and chemical enrichment of CGM/IGM.

It seems that some very high-resolution simulations (\lesssim pc scale) exhibit weaker winds than larger scale simulations that mimic the physics of galactic winds on supergalactic scales (see the contributions by E. Ostriker and C.-G. Kim in this proceedings, and Hu 2019). Although we did not discuss in this article, it will be essential to consider additional physics such as cosmic rays and magnetic fields for more physically plausible models of star formation and feedback (e.g., Hopkins et al. 2022).

It might also be possible to constrain the physics of feedback at larger scales of circumgalactic and intergalactic scales utilizing the Ly α absorption by neutral hydrogen (i.e., the so-called IGM tomography technique) and distribution of metals and dust. For example, Nagamine et al. (2021) have shown that the SN feedback changes the radial distribution of H I gas and the Ly α flux contrast signal at $\sim 30\%$ level. Future comparisons between simulations and the CGM/IGM tomography surveys by WEAVE, MOONS, Subaru PFS, JWST, ELT, and TMT will allow us to further constrain the physics of feedback.

I am grateful to all of my recent collaborators on the research results discussed in this article, including S. Arata, R. Cen, Y. Oku, L. Romano, I. Shimizu, K. Tomida, H. Yajima, and everyone in the AGORA project.

References

- Arata, S., Yajima, H., Nagamine, K., Abe, M., & Khochfar, S. 2020, *MNRAS*, 498, 5541
- Arata, S., Yajima, H., Nagamine, K., Li, Y., & Khochfar, S. 2019, *MNRAS*, 488, 2629
- Becker, G. D., & Bolton, J. S. 2013, *MNRAS*, 436, 1023
- Behroozi, P. S., Wechsler, R. H., & Conroy, C. 2013, *ApJ*, 770, 57
- Bruscoli, M., Ferrara, A., Marri, S., et al. 2003, *MNRAS*, 343, L41
- Cai, Z., Fan, X., Peirani, S., et al. 2016, *ApJ*, 833, 135
- Cai, Z., Fan, X., Bian, F., et al. 2017, *ApJ*, 839, 131
- Cen, R. 2003, *ApJ*, 591, 12
- Cen, R., Miralda-Escudé, J., Ostriker, J. P., & Rauch, M. 1994, *ApJL*, 437, L9
- Cen, R., Nagamine, K., & Ostriker, J. P. 2005, *ApJ*, 635, 86
- Cen, R., & Ostriker, J. P. 1992, *ApJL*, 399, L113
- . 1999, *ApJ*, 514, 1
- Chevalier, R. A. 1974, *ApJ*, 188, 501
- Cowie, L. L., Songaila, A., Kim, T.-S., & Hu, E. M. 1995, *AJ*, 109, 1522
- Croft, R. A. C., Weinberg, D. H., Katz, N., & Hernquist, L. 1998, *ApJ*, 495, 44
- Dalla Vecchia, C., & Schaye, J. 2012, *MNRAS*, 426, 140
- Durier, F., & Dalla Vecchia, C. 2012, *MNRAS*, 419, 465
- Faucher-Giguère, C.-A., Kereš, D., & Ma, C.-P. 2011, *MNRAS*, 417, 2982
- Finkelstein, S. L., D'Aloisio, A., Paardekooper, J.-P., et al. 2019, *ApJ*, 879, 36
- Font-Ribera, A., Arnau, E., Miralda-Escudé, J., et al. 2013, *JCAP*, 5, 018
- Frenk, C. S., White, S. D. M., Bode, P., et al. 1999, *ApJ*, 525, 554
- Fujimoto, S., Ouchi, M., Ferrara, A., et al. 2019, *ApJ*, 887, 107
- Gnedin, N. Y., Kravtsov, A. V., & Chen, H. 2008, *ApJ*, 672, 765
- Greene, J., Bezanson, R., Ouchi, M., Silverman, J., & the PFS Galaxy Evolution Working Group. 2022, arXiv e-prints, arXiv:2206.14908
- Hashimoto, T., Laporte, N., Mawatari, K., et al. 2018, *Nature*, 557, 392
- Hashimoto, T., Inoue, A. K., Mawatari, K., et al. 2019, *PASJ*, 71, 71

- Hernquist, L., Katz, N., Weinberg, D. H., & Miralda-Escudé, J. 1996, *ApJL*, 457, L51
- Hirai, Y., Fujii, M. S., & Saitoh, T. R. 2021, *PASJ*, 73, 1036
- Hopkins, P. F. 2013, *MNRAS*, 428, 2840
- Hopkins, P. F., Butsky, I. S., Panopoulou, G. V., et al. 2022, *MNRAS*, 516, 3470
- Hopkins, P. F., Wetzel, A., Kereš, D., et al. 2018, *MNRAS*, 477, 1578
- Hu, C.-Y. 2019, *MNRAS*, 483, 3363
- Iršič, V., Viel, M., Berg, T. A. M., et al. 2017, *MNRAS*, 466, 4332
- Katz, H., Rosdahl, J., Kimm, T., et al. 2022, *MNRAS*, 510, 5603
- Katz, N. 1992, *ApJ*, 391, 502
- Katz, N., Weinberg, D. H., & Hernquist, L. 1996, *ApJS*, 105, 19
- Kay, S. T., Thomas, P. A., & Theuns, T. 2003, *MNRAS*, 343, 608
- Keller, B. W., Wadsley, J., Benincasa, S. M., & Couchman, H. M. P. 2014, *MNRAS*, 442, 3013
- Kereš, D., Katz, N., Weinberg, D. H., & Davé, R. 2005, *MNRAS*, 363, 2
- Kim, C.-G., & Ostriker, E. C. 2015, *ApJ*, 802, 99
- Kim, C.-G., Ostriker, E. C., & Raileanu, R. 2017, *ApJ*, 834, 25
- Kim, J.-H., Abel, T., Agertz, O., et al. 2014, *ApJS*, 210, 14
- Kim, J.-h., Agertz, O., Teyssier, R., et al. 2016, *ApJ*, 833, 202
- Kimm, T., & Cen, R. 2014, *ApJ*, 788, 121
- Kistler, M. D., Yüksel, H., Beacom, J. F., Hopkins, A. M., & Wyithe, J. S. B. 2009, *ApJL*, 705, L104
- Knebe, A., Pearce, F. R., Thomas, P. A., et al. 2015, *MNRAS*, 451, 4029
- Kollmeier, J. A., Miralda-Escudé, J., Cen, R., & Ostriker, J. P. 2006, *ApJ*, 638, 52
- Kollmeier, J. A., Weinberg, D. H., Davé, R., & Katz, N. 2003, *ApJ*, 594, 75
- Lee, K.-G., Hennawi, J. F., Stark, C., et al. 2014, *ApJL*, 795, L12
- Lee, K.-G., Hennawi, J. F., White, M., et al. 2016, *ApJ*, 817, 160
- Lee, K.-G., Krolewski, A., White, M., et al. 2018, *ApJS*, 237, 31
- Liang, Y., Kashikawa, N., Cai, Z., et al. 2021, *ApJ*, 907, 3
- Ma, X., Quataert, E., Wetzel, A., et al. 2020, arXiv e-prints, arXiv:2003.05945
- Madau, P., & Dickinson, M. 2014, *ARA&A*, 52, 415
- Martizzi, D., Faucher-Giguère, C.-A., & Quataert, E. 2015, *MNRAS*, 450, 504
- McDonald, P., Seljak, U., Burles, S., et al. 2006, *ApJS*, 163, 80
- Meiksin, A., Bolton, J. S., & Puchwein, E. 2017, *MNRAS*, 468, 1893
- Meiksin, A., Bolton, J. S., & Tittley, E. R. 2015, *MNRAS*, 453, 899
- Miralda-Escudé, J., Cen, R., Ostriker, J. P., & Rauch, M. 1996, *ApJ*, 471, 582
- Mukae, S., Ouchi, M., Kakiichi, K., et al. 2017, *ApJ*, 835, 281
- Mukae, S., Ouchi, M., Cai, Z., et al. 2020, *ApJ*, 896, 45
- Nagamine, K. 2018, *The Encyclopedia of Cosmology. Volume 2: Numerical Simulations in Cosmology, Vol. 2* (World Scientific Publishing), doi:10.1142/9496-vol2
- Nagamine, K., Cen, R., Hernquist, L., Ostriker, J. P., & Springel, V. 2004, *ApJ*, 610, 45
- Nagamine, K., Cen, R., & Ostriker, J. P. 2000, *ApJ*, 541, 25
- Nagamine, K., Ostriker, J. P., Fukugita, M., & Cen, R. 2006, *ApJ*, 653, 881
- Nagamine, K., Shimizu, I., Fujita, K., et al. 2021, *ApJ*, 914, 66
- Naidu, R. P., Tacchella, S., Mason, C. A., et al. 2020, *ApJ*, 892, 109
- Nelson, D., Byrohl, C., Peroux, C., Rubin, K. H. R., & Burchett, J. N. 2021, *MNRAS*, 507, 4445
- Nelson, D., Genel, S., Pillepich, A., et al. 2016, *MNRAS*, 460, 2881
- Nicastro, F., Mathur, S., Elvis, M., et al. 2005, *Nature*, 433, 495
- Oku, Y., Tomida, K., Nagamine, K., Shimizu, I., & Cen, R. 2022, *ApJS*, 262, 9
- Ostriker, J. P., & McKee, C. F. 1988, *Reviews of Modern Physics*, 60, 1
- Palanque-Delabrouille, N., Yèche, C., Lesgourgues, J., et al. 2015, *JCAP*, 2015, 045
- Pizzati, E., Ferrara, A., Pallottini, A., et al. 2020, *MNRAS*, 495, 160
- Ploekinger, S., Hensler, G., Recchi, S., Mitchell, N., & Kroupa, P. 2014, *MNRAS*, 437, 3980
- Prochaska, J. X., Hennawi, J. F., Lee, K.-G., et al. 2013, *ApJ*, 776, 136
- Rauch, M. 1998, *ARA&A*, 36, 267
- Razoumov, A. O., & Sommer-Larsen, J. 2006, *ApJL*, 651, L89

- Roca-Fàbrega, S., Kim, J.-H., Hausammann, L., et al. 2021, *ApJ*, 917, 64
- Saitoh, T. R., & Makino, J. 2013, *ApJ*, 768, 44
- Scannapieco, C., Wadepuhl, M., Parry, O. H., et al. 2012, *MNRAS*, 423, 1726
- Schaye, J., Dalla Vecchia, C., Booth, C. M., et al. 2010, *MNRAS*, 402, 1536
- Shimizu, I., Todoroki, K., Yajima, H., & Nagamine, K. 2019, *MNRAS*, 484, 2632
- Shull, J. M., Smith, B. D., & Danforth, C. W. 2012, *ApJ*, 759, 23
- Smit, R., Bouwens, R. J., Carniani, S., et al. 2018, *Nature*, 553, 178
- Smith, B. D., Bryan, G. L., Glover, S. C. O., et al. 2017, *MNRAS*, 466, 2217
- Sorini, D., Davé, R., & Anglés-Alcázar, D. 2020, *MNRAS*, 499, 2760
- Sorini, D., Oñorbe, J., Hennawi, J. F., & Lukić, Z. 2018, *ApJ*, 859, 125
- Springel, V., & Hernquist, L. 2002, *MNRAS*, 333, 649
- . 2003, *MNRAS*, 339, 289
- Stinson, G., Seth, A., Katz, N., et al. 2006, *MNRAS*, 373, 1074
- Takada, M., Ellis, R. S., Chiba, M., et al. 2014, *PASJ*, 66, R1
- Thacker, R. J., & Couchman, H. M. P. 2000, *ApJ*, 545, 728
- Theuns, T., Viel, M., Kay, S., et al. 2002, *ApJL*, 578, L5
- Tillman, M. T., Burkhart, B., Tonnesen, S., et al. 2022, arXiv e-prints, arXiv:2210.02467
- Tomisaka, K., & Ikeuchi, S. 1986, *PASJ*, 38, 697
- Turner, M. L., Schaye, J., Crain, R. A., et al. 2017, *MNRAS*, 471, 690
- Viel, M., Becker, G. D., Bolton, J. S., & Haehnelt, M. G. 2013, *Phys. Rev. D*, 88, 043502
- Viel, M., Lesgourgues, J., Haehnelt, M. G., Matarrese, S., & Riotto, A. 2005, *Phys. Rev. D*, 71, 063534
- Weaver, R., McCray, R., Castor, J., Shapiro, P., & Moore, R. 1977, *ApJ*, 218, 377
- Weinberg, D. H., Burles, S., Croft, R. A. C., et al. 1998, ArXiv Astrophysics e-prints, astro-ph/9810142
- Weymann, R. J., Carswell, R. F., & Smith, M. G. 1981, *ARA&A*, 19, 41
- Wise, J. H., & Cen, R. 2009, *ApJ*, 693, 984
- Wright, R. J., Lagos, C. d. P., Power, C., & Correa, C. A. 2021, *MNRAS*, 504, 5702
- Yajima, H., Nagamine, K., Zhu, Q., Khochfar, S., & Dalla Vecchia, C. 2017, *ApJ*, 846, 30
- Yepes, G., Kates, R., Khokhlov, A., & Klypin, A. 1997, *MNRAS*, 284, 235
- Zabl, J., Bouché, N. F., Schroetter, I., et al. 2020, *MNRAS*, 492, 4576
- Zabl, J., Bouché, N. F., Wisotzki, L., et al. 2021, *MNRAS*, 507, 4294
- Zhang, H., Ouchi, M., Itoh, R., et al. 2020, *ApJ*, 891, 177
- Zhang, Y., Anninos, P., Norman, M. L., & Meiksin, A. 1997, *ApJ*, 485, 496
- Zhang, Y., Meiksin, A., Anninos, P., & Norman, M. L. 1998, *ApJ*, 495, 63